

Recent gullies on Mars and the source of liquid water

Michael T. Mellon and Roger J. Phillips¹

Laboratory for Atmospheric and Space Physics, University of Colorado, Boulder, Colorado, USA

Abstract. Geologic features resembling terrestrial water-carved gullies imply that liquid water has flowed recently on the surface of Mars and challenge our views of the present-day low-temperature environment. We evaluate two possible mechanisms for the formation of liquid water under environmental conditions that we expect to have existed on Mars in its recent past. First, we examine the stability of ground ice in the permafrost and the potential for melting near-surface ground ice (in the top few meters of soil) by solar heating and subsurface conduction. Second, we examine the potential for melting and refreezing of ice at shallow depths due to geothermal heating. We find that near-surface ground ice does not reach the melting point of water under a range of conditions of soil thermophysical properties, latitudes, obliquities, and surface slopes. The atmosphere remains too dry for the ground ice to melt, even at high obliquity; instead, ice sublimates before reaching melting temperatures. However, the presence of salts in concentrations of 15–40% can adequately lower the melting point to allow melting to occur. We also find that a combination of a global average geothermal heat flux and a thick, low-conductivity, unconsolidated regolith raises the depth of the melting isotherm to less than a few hundred meters from the surface. Orbitally induced oscillations in the mean annual surface temperature can cause freezing cycles in a confined aquifer at this depth. Freezing pressures generated are adequate to fracture ice-cemented ground and allow water to escape to the surface, similar to the formation and evolution of terrestrial pingos in shallow permafrost. Both mechanisms are possible; however, the geothermal mechanism is consistent with the observations of the distribution of gullies, while the salty near-surface ground ice mechanism is not. Further observational tests that can be performed with existing and future spacecraft are suggested.

1. Introduction

Observations of geologically young gully landforms in the middle and high latitudes of Mars suggest that liquid water has recently flowed on the surface, yet temperatures are believed to be too low for the source of liquid water to be present at or near the surface in the current climate. Where this water comes from and what these features tell us about Mars remain open questions. In the present work we evaluate two possible mechanisms for the origin of liquid water at the surface of Mars in relation to gully landforms. Both mechanisms involve orbit-induced climate changes causing melting or refreezing of ground ice.

Malin and Edgett [2000] reported geologic features resembling terrestrial water-carved gullies in the middle and high latitudes of Mars. These landforms occur poleward of 30° latitude, primarily in the southern hemisphere. They are found on the walls of impact craters, valleys, graben, and the south polar pits. They are reported more often on poleward facing slopes than on equatorward facing slopes, though they occur on all orientations of slopes. The morphology of the gullies varies but typically consists of a source region “alcove” of order 100 m in size, v-shaped channels of order 10 m wide leading from the alcove, and a depositional fan at the base (see Figure 1). The source regions appear to originate a few hundred meters or less from the top of the local slope and are

frequently associated with exposed strata of material that appears to exhibit cohesive strength, as evidenced by overhangs and eroded blocks. Erosion is best explained by a fluid of some sort, and water is considered the most likely candidate [*Malin and Edgett*, 2000]. *Malin and Edgett* [2000] estimate that a minimum of roughly 2500 m³ of water is needed to form each gully. These features are believed to be geologically young by their superposition atop dunes and permafrost polygons; how young is difficult to determine, though a range of older than 20 years to younger than 1 Myr is suggested.

The general understanding of the current Martian climate has been that the planet is globally covered with permafrost. Permafrost consisting of porous soil in diffusive contact with the atmosphere is expected to be ice-rich at middle and high latitudes due to condensation of atmospheric water vapor. At these latitudes the average soil temperatures are below 196 K, the average saturation temperature of atmospheric water vapor or atmospheric frost point, and ground ice is stable with respect to sublimation [*Leighton and Murray*, 1966; *Farmer and Doms*, 1979; *Fanale et al.*, 1986; *Zent et al.*, 1986; *Paige*, 1992; *Mellon and Jakosky*, 1993]. Mars also undergoes orbital oscillations [e.g., *Ward*, 1974; *Bills*, 1990] that can significantly alter the climate [e.g., *Toon et al.*, 1980]. At higher obliquities than the present, the polar regions become warmer, resulting in more sublimation from the polar caps and higher atmospheric water vapor concentrations; combined with lower equatorial soil temperatures, the near-surface permafrost can become periodically ice-rich at all latitudes at moderately high obliquities, though permanent ground ice is expected only poleward of 30°–40° [*Mellon and Jakosky*, 1995].

In regions where ground ice is stable, densely ice-cemented soil should occur below a few tens of centimeters of dry soil, a boundary we term the “ice table.” Below the ice table the soil

¹On sabbatical leave from McDonnell Center for the Space Sciences and Department of Earth and Planetary Sciences, Washington University, St. Louis, Missouri, USA.

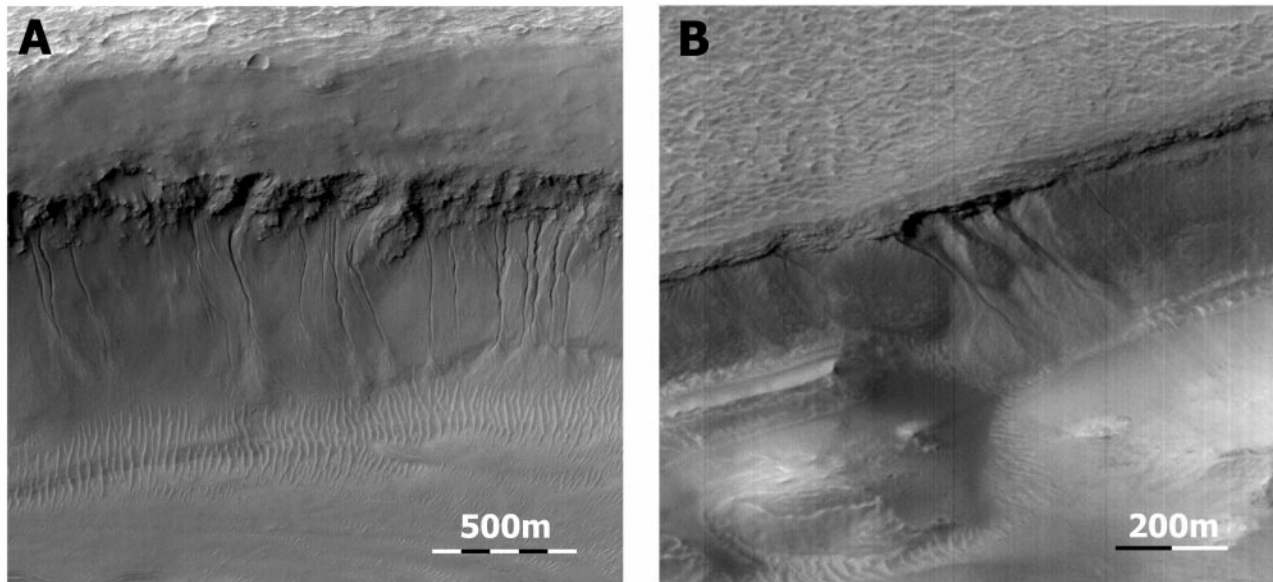


Figure 1. Images of gullies on Mars: (a) on the wall of Nirgal Vallis near $29.7^{\circ}\text{S} \times 39^{\circ}\text{W}$, subframe of Mars Orbiter Camera (MOC) image M03-02290, and (b) in a valley in Gorgonum Chaos near $38.5^{\circ}\text{S} \times 171.5^{\circ}\text{W}$, subframe of MOC image M07-02909. Gully features frequently appear to stem from or below cohesive strata exposed along the slope.

will become ice-cemented to a depth of several meters (the depth of penetration of the seasonal thermal wave, which aids in the transport of water vapor) [e.g., *Mellon and Jakosky*, 1993]. Deeper still, ground ice could exist if subsurface water vapor diffuses toward the surface, down the geothermal gradient [e.g., *Clifford*, 1990], to condense as ice at this coldest, shallow depth. If a substantial groundwater supply existed, water ice could collect within the permafrost, filling it completely [e.g., *Clifford*, 1993; *Mellon et al.*, 1997]. In the absence of deeper sources of water, however, the regolith below several meters could remain ice-free. The depth of the base of the permafrost is controlled by the mean surface temperature, geothermal heating, and the conductivity of the overlying soil, frequently assumed to be ice-cemented; estimates of this depth are shallowest near the equator, where surface temperatures are warmest, and are several kilometers or more near the poles [Rossbacher and Judson, 1981; Kuzmin, 1983; Clifford, 1993; *Mellon et al.*, 1997].

The distribution of gully features coincides with the expected distribution of near-surface ground ice [Mellon and Jakosky, 1995], suggesting a possible genetic relationship. The larger abundance of gullies on poleward facing slopes also suggests that patterns of solar heating may play a role [Malin and Edgett, 2000]. However, the low ground temperature at the latitudes at which the gullies are found presents a contradiction to the presence of liquid water. In this work we consider two potential sources for liquid water. First, we consider whether near-surface ground ice (ice in the top few meters of soil) can melt under special climatic or geologic conditions. Specifically, we evaluate the effects of surface slope, latitude, orbital changes, and thermophysical properties of the soil and the transient effects of erosion. Second, we consider whether reasonable conditions can occur for geothermal heat to adequately warm the subsurface, such that pockets of liquid water may exist at depths shallower than previously considered. In this work we apply standard numerical models of soil temperatures on Mars and the stability of ground ice.

In the following section we discuss central issues regarding the Martian orbit and its effect on the Martian climate. We will then describe two models for potential sources of liquid water,

discuss their implications, and suggest observational tests of these scenarios.

2. Mars' Orbit and Its Effect on Climate

Mars is known to undergo large oscillations in its orbit, due to periodic forcing from the Sun and other planets [e.g., *Ward*, 1974], which have a pronounced influence on its climate [e.g., *Toon et al.*, 1980]. Of particular interest are the obliquity (tilt of the spin axis relative to the orbit plane), the eccentricity, and the L_S at perihelion (the areocentric longitude of the Sun or season at which perihelion occurs). Of these, obliquity has the largest effect on the Martian climate and surface temperature. At obliquities higher than the present 25.19° , more solar energy reaches the polar caps, which in turn increases the temperature and sublimation rate of surface ice [Toon et al., 1980; *Jakosky et al.*, 1993, 1995] and the quantity of atmospheric water vapor. Similarly, changes in obliquity and the other orbital elements change the planetwide distribution of solar heating of the soil surface.

The Martian orbital history is determined here using a linear perturbation model [Ward, 1974; Bills, 1990] combined with secular Fourier components from *Laskar* [1988]. Using an updated axial precession rate determined from the Pathfinder Lander radio tracking data [Folkner et al., 1997] of 8.268 ± 0.040 arc sec yr^{-1} , Figure 2 shows the history of the Martian orbit for the past 10^7 years. At this axial precession rate the obliquity varies from about 11° to 40° . Despite the remaining uncertainty in the precession rate, the obliquity history remains fairly certain, since this rate does not fall near a secular resonance [Bills, 1990]. However, on timescales longer than 10^7 years the behavior of the orbits of all the inner planets was found to be chaotic [Laskar, 1989], and the obliquity of Mars could experience excursions from as low as 0° to as high as 60° through variations in the long-term mean obliquity [Laskar and Robutel, 1993; Touma and Wisdom, 1993]. While the mean obliquity and the exact phase of the oscillations are inherently unpredictable, the general behavior illustrated in Figure 2 is

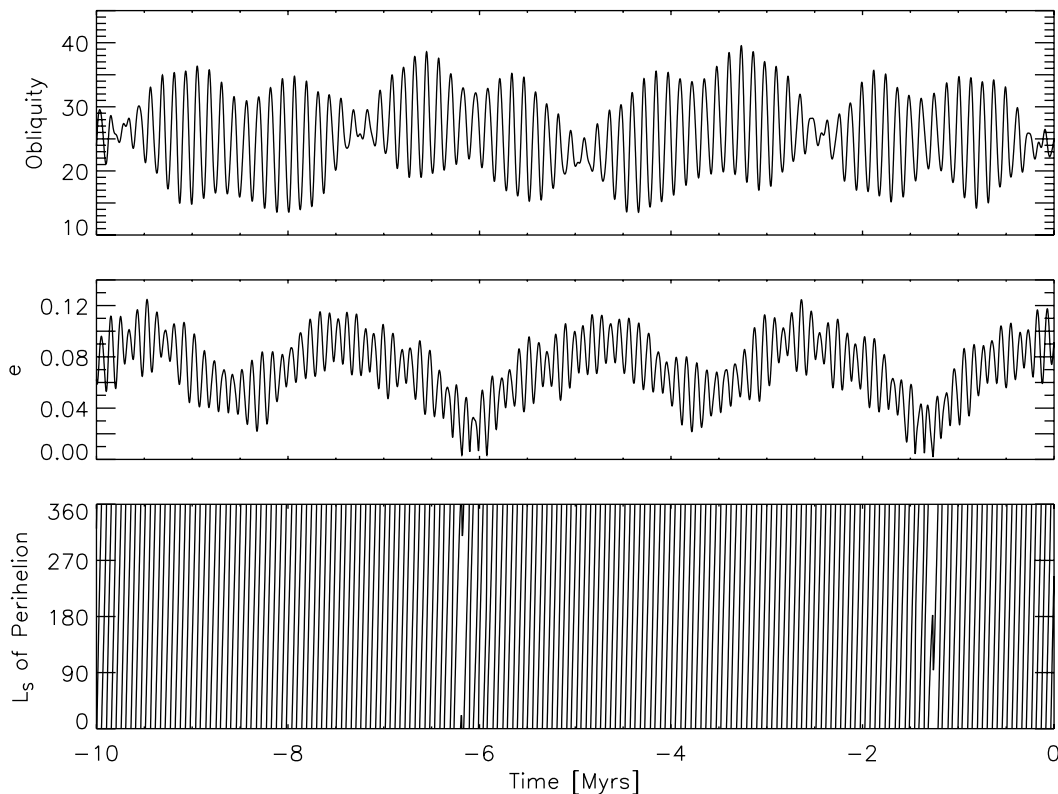


Figure 2. Mars orbit history for the past 10 Myr, assuming an axial precession rate of $8.268 \text{ arc sec yr}^{-1}$ based on new Pathfinder tracking results. Shown are typical oscillations for obliquity, eccentricity, and L_S of perihelion. Prior to 10 Myr ago the orbit becomes increasingly unpredictable, though the style of oscillations shown is representative of longer timescales.

representative of longer timescales, where obliquity can increase by nearly 20° in as little as 60,000 years. Since the exact age of gully features is unknown, we will consider the orbital history on timescales longer than 1 Myr and possible excursions to extreme values.

The Martian surface temperatures vary considerably with changes in obliquity. Figure 3 shows the mean annual surface temperature as a function of latitude for a variety of obliquities assuming average surface properties for Mars. The model used to calculate these temperatures will be discussed in the next section,

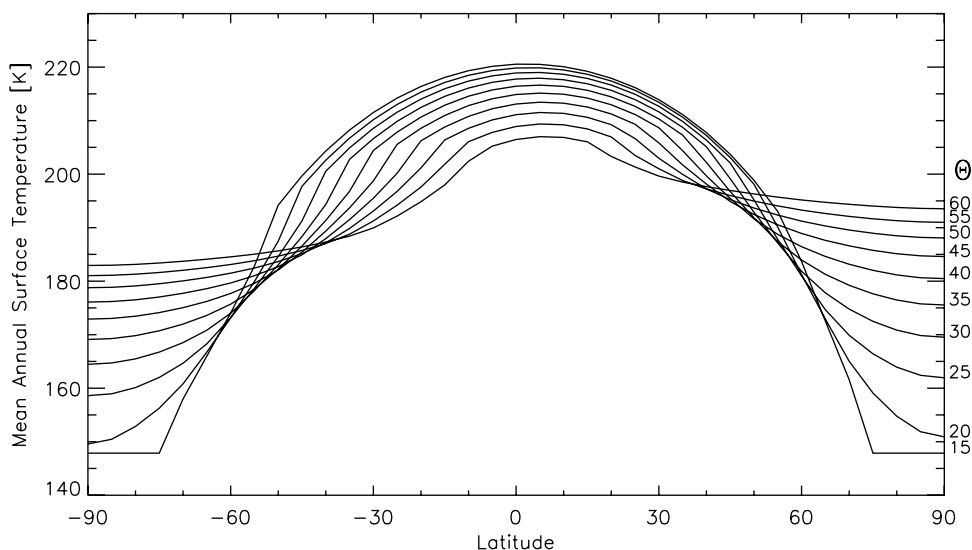


Figure 3. Mean annual surface temperature for a range of obliquities. The eccentricity is 0.12, and the L_S at which perihelion occurs is 270, corresponding to southern summer. A thermal inertia of $250 \text{ J m}^{-2} \text{ s}^{-1/2} \text{ K}^{-1}$, an albedo of 0.25, a surface pressure of 600 Pa, and an infrared dust opacity of 0.1 are assumed. Discontinuities in the slope of each curve are due to the effects of seasonal CO_2 frost.

but it is worth noting at this point that the mean temperatures do not exceed 222 K for any latitude and are colder still for the latitudes at which gullies are observed. Special conditions are therefore required in order for liquid water to be generated at or near the surface.

An important boundary condition for ground ice stability is the average amount of water in the atmosphere. At the present epoch the average water vapor abundance in the Martian atmosphere is observed to be ~ 10 precipitable micrometers (pr μm) [Jakosky and Farmer, 1982; Jakosky and Barker, 1984]. This quantity of water results primarily from exchange of water with the seasonal and residual polar caps and meridional transport to and from nonpolar latitudes [Haberle and Jakosky, 1991]. For the quantity of atmospheric water at obliquities other than the present one we adopt the model of Mellon and Jakosky [1995] shown in Figure 4. In this model the increase or decrease in sublimation of water from the polar caps as a function of obliquity [Jakosky et al., 1993, 1995] is assumed to correlate with the same magnitude increase or decrease in the abundance of water vapor in the atmosphere (see Mellon and Jakosky [1995] for additional discussion).

3. Near-Surface Ground Ice Stability

3.1. Problem and Model

In this section we will consider the potential melting of near-surface ground ice (ice in the top several meters of soil) and evaluate climatic, geographic, and thermophysical conditions which may be favorable to formation of liquid water. We will focus primarily on three situations where melting might occur: (1) ice at the ice table (depth of transition from relatively ice-free soil to densely ice-cemented soil) is warmed by solar heating and thermal conduction from the surface; (2) trace quantities of seasonal ice above the ice table are warmed prior to sublimation; and (3) erosion exposes the ice table to direct solar heating. In each of these cases we employ a standard numerical model of surface and subsurface temperatures and of water transport and ice stability, with a few modifications as described below. The thermal model [Haberle and Jakosky, 1991; Mellon et al., 2000] accounts for solar heating, CO_2 surface frost, thermal radiation to space, and subsurface conduction and includes the radiative effects of a dusty, CO_2 atmosphere. Subsurface temperatures are calculated by a forward-time finite difference solution to the

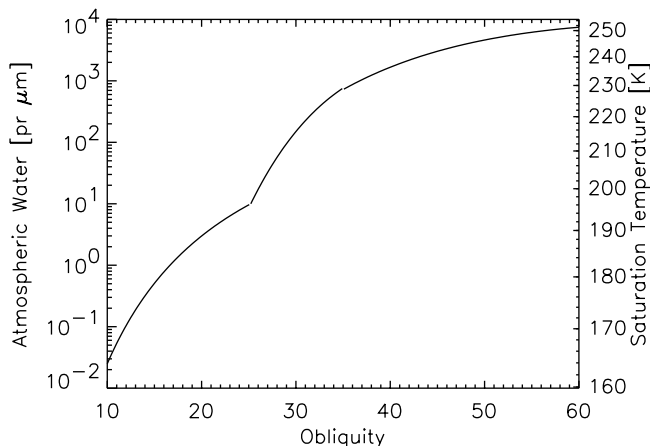


Figure 4. Average atmospheric water column abundance and surface saturation temperature as a function of obliquity from Mellon and Jakosky [1995], based on calculated rates of summertime sublimation from the polar ice deposits [Jakosky et al., 1993, 1995]. Above the present obliquity the atmospheric pressure is assumed constant at the present-day value, accounting for the discontinuity in the slope of the curve at 25.19°.

thermal diffusion equation with this surface boundary condition and a nonconducting boundary at a depth well below solar influences. Water transport and ground ice stability are found by a similar solution to the molecular diffusion equation and phase partitioning of water [Mellon and Jakosky, 1993], utilizing calculated subsurface temperatures and boundary conditions of atmospheric water vapor at the surface and a nondiffusive boundary well below depths of interest. Temperatures and water transport are solved throughout the Martian day and year. The present model does not account for spatial or temporal variability in the subsurface thermal properties, such as caused by ice cement in the soil. Our aim is to place limits on the conditions for which melting temperatures could be reached; as such, we test a range of thermal properties.

The effects of local surface slopes have been included. Observed gullies occur on a variety of surfaces [Malin and Edgett, 2000], some exhibiting substantial cohesive strength apparent from exposed strata. The angle of repose is typically around 35° for unconsolidated materials; however, gullies might originate on loose surfaces of lower slope angle or on cohesive surfaces of higher slope angles. We therefore consider slopes in our model of 0°, 20°, 40°, and 60° facing in poleward and equatorward directions. We do not consider east-west facing slopes in the present work. To determine the effect of slopes, we model a slope surface next to an adjacent level plane, which is considered to extend infinitely away from the slope; in this configuration the relative elevation along the slope above the plane is unimportant. We first compute the seasonal surface temperatures and incident solar radiation for a level surface. We then use these results to determine the quantity of radiated thermal energy and reflected solar energy incident on the slope surface from the adjacent plane. The direct incident solar flux at the slope surface is

$$F_i = \left(\frac{S}{R^2} - F_{\text{CO}_2} \right) \mu_\alpha e^{-\tau/\mu}, \quad (1)$$

where S is the solar constant at Earth, R is the Martian orbital radius in AU, F_{CO_2} is the amount of solar flux absorbed by CO_2 determined by integration through the atmosphere, μ_α is the cosine of the solar incidence angle at the slope α (measure from the zenith), μ is the cosine of the solar incidence angle on a level surface, and τ is the dust opacity. Solar zenith angles will depend also on the latitude, time of day, season, and obliquity. For all the models we assume a 600 Pa CO_2 surface pressure and an infrared dust opacity of 0.1; normal variations in these parameters should not significantly affect the results. When the Sun is below the horizons for either the local level surface or the slope surface, F_i is set to zero. For the diffuse component of the solar flux and the downwelling atmospheric infrared radiation, the values for a level surface are modified by the factor $1/2[1 + \cos(\alpha)]$, which accounts for the average incidence angle of the sky onto the surface. The absorbed solar radiation reflected from the adjacent plane is given by

$$F_{\text{vis}} = (1 - A_\alpha) A_0 F_S 1/2 [1 - \cos(\alpha)], \quad (2)$$

and the absorbed infrared radiation emitted by the adjacent plane is given by

$$F_{\text{IR}} = \varepsilon_\alpha \varepsilon_0 \sigma T_0^4 1/2 [1 - \cos(\alpha)], \quad (3)$$

where F_S is the incident solar flux on a level surface, A is the albedo, ε is the infrared emissivity, T is the surface temperature, and the subscripts α and 0 indicate the slope surface and the adjacent plane, respectively. The factor $1/2[1 - \cos(\alpha)]$ accounts for the mean incidence angle of the plane onto the slope.

To evaluate the effects of changes in obliquity, we divide an orbital history into 5000 year epochs. Starting at 24.7°, we ramp

Table 1. Solar Heating of Ground Ice: Model Parameters

Property	Parameter	Value	Units
Thermal inertia ^a	I	250	$\text{J m}^{-2} \text{s}^{-1/2} \text{K}^{-1}$
Albedo ^a	A	0.25	
Density ^b	ρ	1650	kg m^{-3}
Specific heat	C	837	$\text{J kg}^{-1} \text{K}^{-1}$
Porosity ^b	ϵ_0	0.4	
Pore radius	r_0	10	μm
Tortuosity	τ_0	3	

^aApproximate global average values for Mars [Mellon *et al.*, 2000].

^bChosen to be consistent with surface soil densities estimated from radar and Viking Lander data [Moore *et al.*, 1987]; other parameters are estimates commonly used in ground ice stability models [see Mellon and Jakosky, 1993].

the obliquity down to 19.5° and back up as it would over a natural cycle. When the maximum rate of increasing obliquity is reached, $\sim 2.5^\circ$ per epoch, that rate is held to a maximum obliquity of 55° . The eccentricity is 0.12 and the L_S of perihelion is 270 at all times to maximize summer heating in the southern hemisphere. Initially, ice is set to occupy 75% of the pore space in the regolith at all depths and is allowed to exchange with the atmosphere as stability conditions and rates of diffusion dictate. This initial ice content

was chosen to maximize the availability of ice yet provide some open pores for diffusion to occur between lower layers. The obliquity history chosen allows the ice content to relax to a minimum at low obliquity, when the atmosphere is driest, so that the depth to the ice table and ice content respond to a natural increase in the obliquity. In this way we avoid placing ice artificially at depths where it would not naturally occur. The first 40 kyr are discarded to avoid the effects of these initial conditions, and the remaining results are saved for obliquities from 20° to 55° .

3.2. Results

We ran three simulations for 30° , 50° , and 70° south latitude (commensurate with the distribution of gullies). In each case, average Martian thermal properties and nominal diffusive properties for unconsolidated soils were used; Table 1 contains a list of model parameters. Later, we will vary these parameters to test extreme conditions. Figure 5 shows the resulting average and maximum annual surface temperature as a function of slope and obliquity. Generally, annual average temperatures on poleward facing slopes are coldest and equatorward facing slopes are warmest, with the coldest slope being 40° poleward. Annual average temperatures, also representative of the subsurface, are all well below the melting point of pure water, 273 K. While maximum surface temperatures can exceed the melting point, ice is not present.

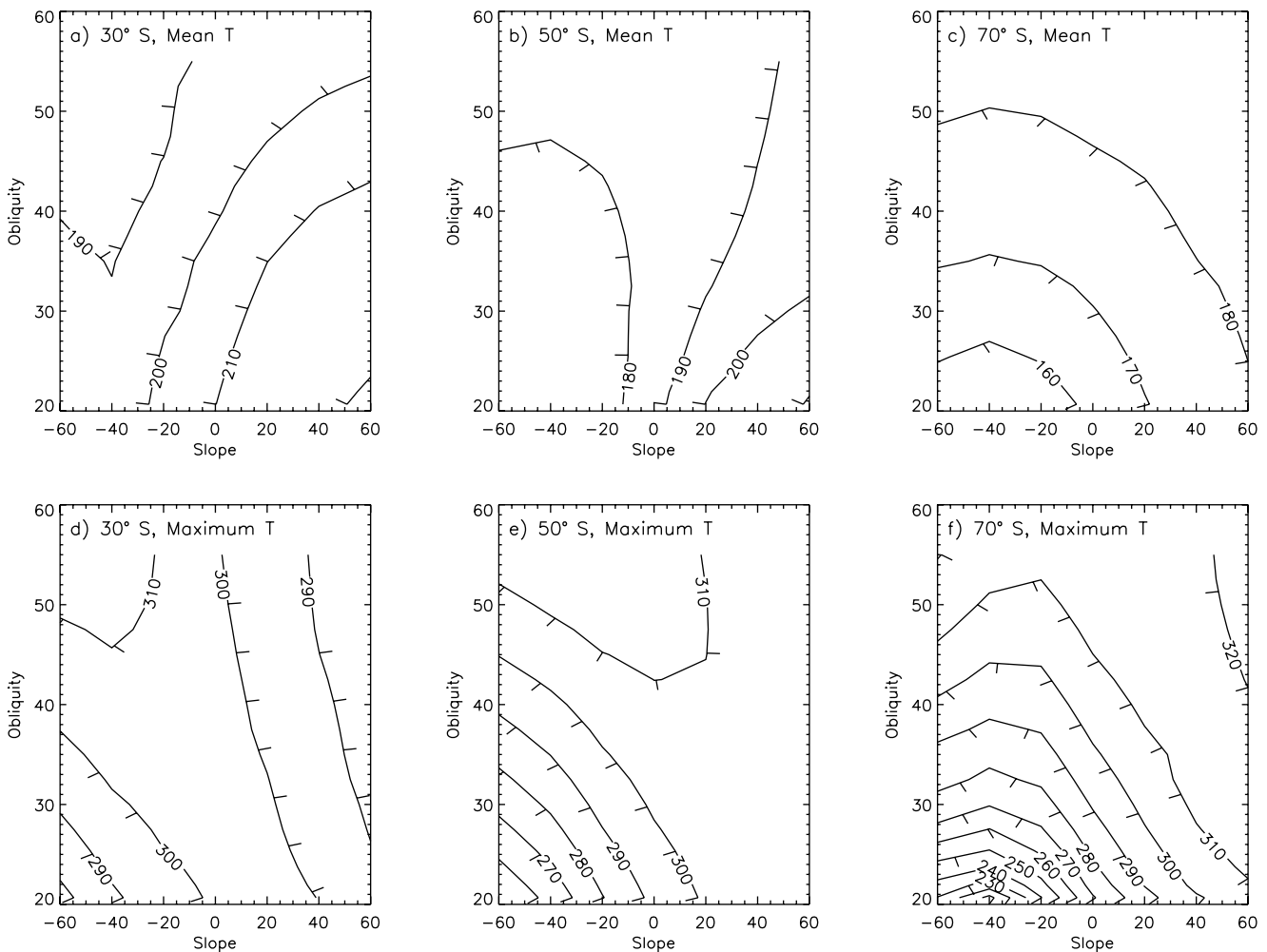


Figure 5. Contours of (a–c) the mean annual surface temperature and (d–f) maximum annual surface temperature as a function of obliquity and surface slope for latitudes of 30° , 50° , and 70° south. The eccentricity was 0.12, and L_S of perihelion was 270. Thermophysical properties of the surface are given in Table 1. Slope angles are northward; therefore negative slopes are poleward at these latitudes. Contours are at 10 K intervals.

Figure 6 shows the depth to the ice table and the maximum annual temperature experienced by ice at that depth. Above the ice table, trace amounts of water persist during only parts of the year, and the soil is otherwise ice-free. At and below the ice table the permafrost is ice-cemented. The transition is relatively abrupt, within one model layer [see also *Mellon and Jakosky*, 1993, 1995]. The depth to the ice table varies substantially with slope and obliquity being generally shallowest on the colder poleward facing slopes. In contrast, the maximum temperature experienced by ice at the ice table is relatively insensitive to the surface slope and latitude. Smaller variations are mainly due to discrete steps in the depth of the ice table from finite model layers. At obliquities greater than $\sim 30^\circ$, maximum temperatures are nearly the same as the saturation temperature of atmospheric water vapor (Figure 4). The depth of the ice is controlled by this boundary condition, so that as the climate changes, the ice depth moves up or down coincident with the atmospheric frost point. At warmer temperatures, water diffuses more rapidly than at cooler temperatures due to the exponential

dependence of the saturation pressure on temperature; thus equilibrium is dominated by the warmer temperatures. At obliquities lower than 30° , where ice is deeper and colder, diffusion of water vapor is slow and the correlation is not as strong.

We also conducted a simulation at 50° south latitude with a higher thermal inertia of $790 \text{ J m}^{-2} \text{ s}^{-1/2} \text{ K}^{-1}$ and a lower albedo of 0.15 to aid in conducting more heat to depth. In addition, we included a lower porosity of 15%, a smaller pore radius of $1 \mu\text{m}$, and higher tortuosity of 6 to retard water movement and sublimation as temperatures rise. These parameters are roughly consistent with a consolidate material like a weakly cemented sandstone. While the ice table is generally more than two times deeper, the resulting maximum temperatures at the ice table were similar to Figure 6, indicating a minimal dependence on these factors and supporting a primary dependence on the atmospheric frost point.

Seasonally, small quantities of ice occur in the relatively dry soil above the ice table. This ice condenses during the coldest seasons and rapidly sublimates when heated. The amount of ice that occurs

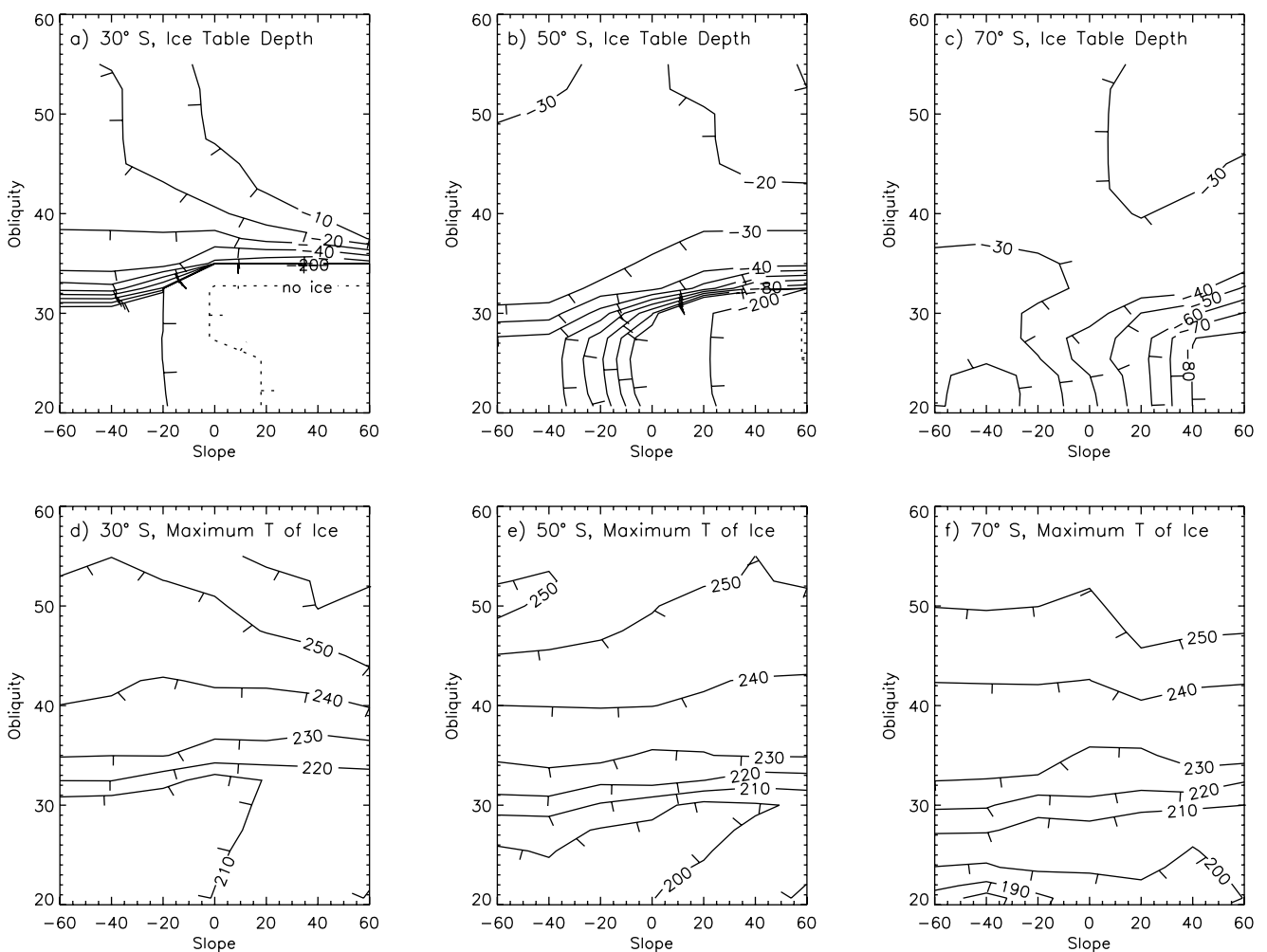


Figure 6. Contours of (a–c) the depth of the ice table and (d–f) the maximum annual temperature experienced by the ice at this depth. The ice table represents an abrupt transition from ice-free soil above to densely ice-cemented soil below. Only trace quantities of ice occur seasonally above the ice table, which completely sublimates in summer. We specifically define this transition as the depth where ice content exceeds 50% of the pore space between discrete model layers. The maximum temperatures are relatively uniform in slope and latitude and are similar to the atmospheric saturation temperature, indicating that this is an important boundary condition. Contour intervals are 10, 20, 30, 40, 50, 60, 70, 80, 90, 100, and 200 cm below the surface for the depth of the ice table. “No ice” marks the transition from ground ice stability to instability. Temperature contours are at 10 K intervals. While the first 40 kyr have been discarded to avoid the effects of the initial ice distribution, these effects are still apparent at lower latitudes of 30° and 50° , up to obliquities of 30° and 25° , respectively. However, the results at higher obliquities and the overall conclusions are unaltered.

varies from typically $10\text{--}20\text{ mg cm}^{-3}$ to occasionally more than 100 mg cm^{-3} for low-latitude, high-obliquity, equatorward-slope models. For a porosity of 40% the regolith becomes ice-saturated at 370 mg cm^{-3} . As with the maximum temperatures of the ice table, the maximum temperatures experienced by this seasonal ice above the ice table do not reach the melting point. Temperatures can get above 260 K only at the obliquities above 42° ; when these higher temperatures are reached, $\sim 5\text{--}20\text{ mg cm}^{-3}$ of sublimating ice remains for brief periods, depending on obliquity, slope, and latitude. For comparison, water adsorbed on the surface of the soil grains amounts to $5\text{--}15\text{ mg cm}^{-3}$, depending on the temperature; even if these quantities of ice were to melt, they would barely wet the soil and be incapable of causing the observed soil erosion.

Finally, we considered the effect of an erosional process removing the dry soil above the ice table, exposing ice-cemented soil directly to solar heating. The dry soil above the ice table could be removed by wind or slumping. To evaluate this effect, we conducted a series of simple numerical simulations where ice-saturated soil was instantly exposed at the surface with the initial temperature that it possessed at depth prior to exposure. The exposed ice-cemented soil was then allowed to receive direct solar heating and exchange water with the atmosphere for one Mars year. Simulations were conducted for obliquities of 25.4° , 40° , and 55° and a latitude of 50°S . Local slope, albedo, and thermal inertia were varied to test for favorable conditions for melting. We considered a range of thermal inertias from 250 to $2000\text{ J m}^{-2}\text{ s}^{-1/2}\text{ K}^{-1}$; the higher values are consistent with ice-cemented soil, while the lower values are consistent with a dry soil layer that might blanket the ice if the first few layers desiccate. Results indicate that the ice quickly sublimates and the regolith becomes desiccated to a depth of $5\text{--}10\text{ cm}$, before melting temperatures could be reached. The warmest temperatures experienced by the top of the receding ice table were typically $\sim 265\text{ K}$. In practice, the high thermal conductivity of ice-cemented soil should more efficiently transport heat away from the surface, maintaining low temperatures.

3.3. Discussion on Near-Surface Ground Ice

Generally, our model results indicate that even under the most optimistic conditions, near-surface ground ice cannot reach the melting point of pure water (273 K) by solar heating alone. It may be possible, however, for ice to melt at the lower temperatures found if salt is present in the ice-rich permafrost. Salt has been inferred to be present in the regolith on Mars due to the observations of duricrust (weakly cohesive soil material) at the Viking and Pathfinder landing sites [Mutch *et al.*, 1977; Binder *et al.*, 1977; Moore *et al.*, 1999]. A high abundance of sulfur and chlorine and the detection of bromine in the soil suggest that sulfate, chloride, and bromide salts may be present [Clark *et al.*, 1982; Rieder *et al.*, 1997]; although other salts may be present, including carbonates and nitrates, these ions were not measured [Clark and van Hart, 1981; Rieder *et al.*, 1997]. There is also a remarkable uniformity in the concentration of salt-forming ions between these landing sites. Brass [1980] examined the eutectic temperatures of various brine compositions and found that the freezing point could be depressed to as low as 223 K and lower still if more than one salt species is present, but the concentrations of salts required are very high. Figure 7 shows the freezing point depression of brine solutions for a selection of salt species that may occur on Mars. Given the temperatures that occur at the ice table (e.g., Figure 6), the concentration of salt required for melting to occur varies from about 15% to 40% by weight, depending on the salt species and temperature. For comparison, terrestrial seawater contains $\sim 3.5\%$ salt by weight and freezes at $\sim 271.3\text{ K}$ [Horne, 1969].

While such high salt concentrations are possible, the question remains as to whether they are likely. Kuzmin and Zabalueva [1998] suggested that brine pockets can occur in the Martian permafrost, allowing high concentrations to build as salts are rejected from the gradually freezing solutions. However, such high

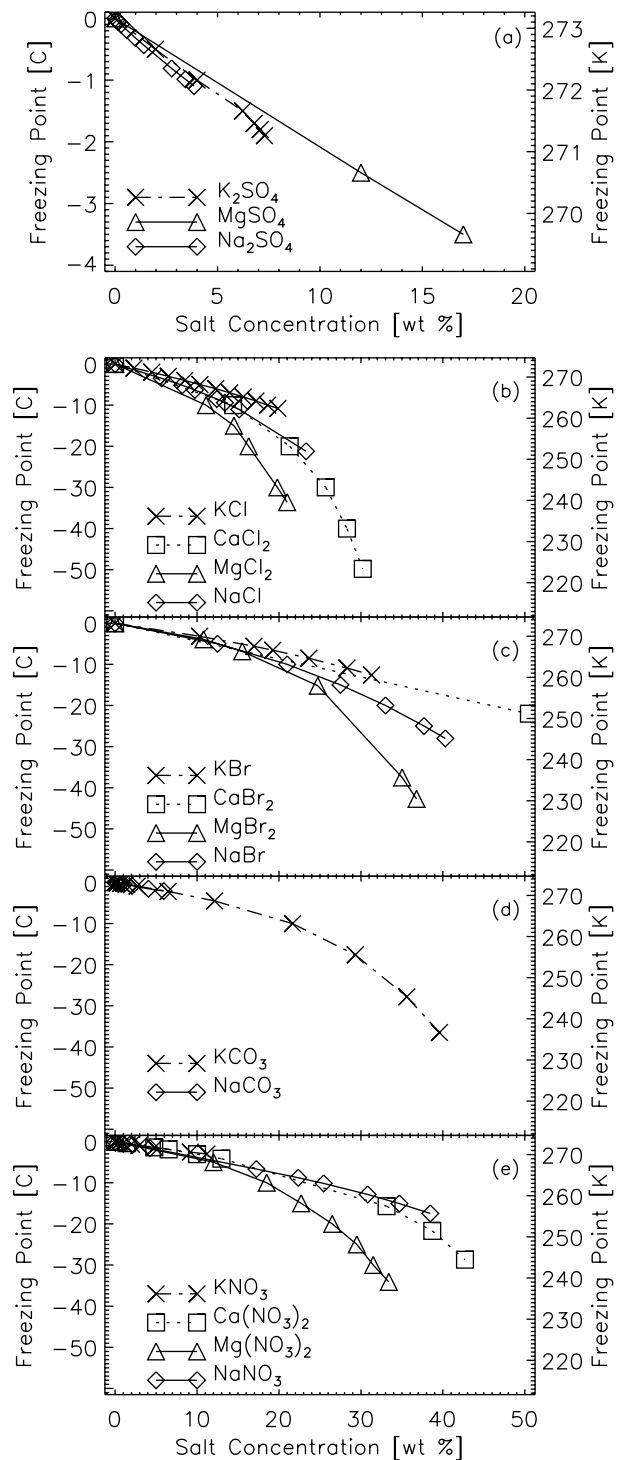


Figure 7. Freezing point depression of water as a function of salt concentration for a variety of salt species: (a) sulfates, (b) chlorides, (c) bromides, (d) carbonates, and (e) nitrates. Sulfates are least capable of depressing the freezing point, even at high concentrations, while chlorides are most effective. Data are from Linke [1958], with data from Hall and Sherrill [1928] for carbonates, NaSO_4 , and KNO_3 . The lowest freezing points given are the eutectics for each salt.

concentrations have not yet been observed. Clark and van Hart [1981] estimated abundances of 8% to 15% sulfates and 0.5% to 1.5% chlorides and trace bromides at the Viking landing sites from the measured abundances of salt-forming ions. If these abundances

of salts are present in the ice-rich permafrost, they are unlikely to depress the freezing point more than a few degrees [see also *Kuzmin and Zabalueva*, 1998]. In addition, the water responsible for forming gullies appears to discharge from a specific depth or depths along each slope a few hundred meters or less from the top, frequently in association with or below exposed strata (see Figure 1). A confined salt deposit might result in ground ice preferentially melting at a narrow band below the top of the slope, though such a salt deposit could occur at any depth and not be limited to a few hundred meters below the top of the slope. Ground ice should be present at all elevations along the slope as well as on level surfaces, and exposure of a salt deposit would cause melting in all these locations. Ultimately, salty meltwater would be washed down the slope and be deposited at the base of each gully. Since the subsurface below a few centimeters' depth is expected to be ice saturated, the salt solution would not be able to percolate far into the ground. Evaporite deposits of salts would remain at the surface, where they may be visible.

Throughout these simulations the atmospheric water abundance has proven to be an important boundary condition. The model used here is an approximation based on simple sublimation into a dry CO₂ atmosphere [*Jakosky et al.*, 1993]. We do not know exactly what the atmospheric water cycle is at higher obliquities; indeed, the water cycle at the current epoch is not fully understood. The true quantity of atmospheric water may be larger or smaller than assumed here. For example, higher vapor concentrations might be due to lower polar cap albedo from a thin dust deposit raising the surface temperature and sublimation rate, while lower concentrations might be due to higher CO₂ pressures, high atmospheric humidity locally over the cap, or the formation of a thick dust lag deposit, all of which would retard sublimation. Since the maximum temperature of the ice table and the atmospheric frost temperature are closely correlated, for ground ice to persist at sufficiently shallow depths to melt would require the atmosphere to saturate at or above the melting temperature. In this case the atmosphere would need to be at or above 273 K and would hold enough water that liquid precipitation would be likely; however, gully images indicate undermining erosion and collapse along a confined zone, indicative of subsurface seepage [*Malin and Edgett*, 2000].

4. Geothermal Heating and Liquid Water

In this section we describe a simple model of the temperature profile in the deeper Martian subsurface (of order a few hundred meters) and evaluate the potential for liquid water due to nominal geothermal heating. Many of the observed gully landforms appear to have source regions stemming from (possibly just below) exposed strata exhibiting some cohesive strength (see Figure 1). These strata and source regions are exposed a few hundred meters or less below the top of the slope [*Malin and Edgett*, 2000]. We evaluate what geophysical conditions are necessary for liquid water to occur at these shallow depths from geothermal energy and the potential for discharge of water at the surface.

The conductive temperature profile in the subsurface caused by geothermal heat alone is given by Fourier's law:

$$\frac{\partial T}{\partial Z} = \frac{q}{k}, \quad (4)$$

where T is the subsurface temperature at depth Z , q is the geothermal heat flow, and k is the thermal conductivity. The geothermal heat flow of Mars has not yet been measured. However, theoretical models of the planet's interior thermal evolution suggest the global-mean surface heat flow is in the range of 20–45 mW m⁻² for the present day [*Johnston et al.*, 1974; *Fanale*, 1976; *Toksöz and Hsui*, 1978; *Toksöz et al.*, 1978; *Turcotte et al.*, 1979; *Davies and Arvidson*, 1981; *Stevenson et al.*, 1983; *Franck and Orgzall*, 1987; *Schubert and Spohn*, 1990; *Spohn*, 1991; *Schubert*

et al., 1992]. An intermediate value of 30 mW m⁻² is frequently used, and we adopt this value in the present work. Integration of (4) yields,

$$T(Z) = T_S + \int_0^Z \frac{q}{k(Z')} dZ', \quad (5)$$

where T_S is the mean surface temperature. Similarly, we can express the lithostatic pressure as

$$P(Z) = P_S + \int_0^Z \rho(Z') g dZ', \quad (6)$$

where P_S is the surface atmospheric pressure (600 Pa), ρ is the soil density, and g is Mars surface gravity, 3.73 m s⁻².

Previous studies that considered the depth of the melting isotherm used a regolith thermal conductivity consistent with ice-cemented soil or basaltic rock [*Rossbacher and Judson*, 1981; *Kuzmin*, 1983; *Clifford*, 1993; *Mellon et al.*, 1997]. However, the thermal conductivity of the Martian regolith at depths of a few hundred meters is unknown. Observations of the surface temperature of Mars have been used to determine the thermal inertia of the surface layer (top few centimeters) [e.g., *Palluconi and Kieffer*, 1981; *Mellon et al.*, 2000]. A global average value of 250 J m⁻² s^{-1/2} K⁻¹ is typical of the southern midlatitudes, and assuming a density and specific heat (see Table 1), this translates to a thermal conductivity of ~0.045 W m⁻¹ K⁻¹, consistent with a dry particulate soil where gas conduction dominates the heat transfer [e.g., *Presley and Christensen*, 1997a]. Below the surface many processes can act to raise the thermal conductivity: ice cementing, densification, lithostatic compression, and induration. If the soil below a few meters' depth (the seasonal thermally active layer) is in diffusive contact with a deeper source of water such as a groundwater table, water vapor will diffuse upward following the geothermal gradient and condense [*Clifford*, 1990], ultimately saturating the coldest shallow depths of the permafrost with ice. Densely ice-cemented soil would have a thermal conductivity of ~2.4 W m⁻¹ K⁻¹, depending on the ice-to-soil ratio and the temperature. If the regolith grains are ice-free but indurated, the thermal conductivity would still increase significantly due to the enhancement of the conductive contacts between the grains. As an example, a dry terrestrial sandstone has a conductivity of around 0.9 W m⁻¹ K⁻¹ or higher [*Roy et al.*, 1989]; lower values would be expected at lower gas pressures, consistent with Martian atmospheric pressure [e.g., *Woodside and Messmer*, 1961].

To illustrate the dependence on material properties, Figure 8 shows, superimposed on the phase diagram of water, the geothermal gradient from (5) and (6) for constant values of thermal conductivity and density consistent with an ice-cemented soil, an ice-free sandstone, and an ice-free soil. A constant mean annual surface temperature of 180 K was assumed. The depth at which the melting point is achieved is strongly dependent on the thermal conductivity, primarily because thermal conductivity can vary by orders of magnitude between geologic materials; uncertainties in other parameters such as heat flow are secondary. For high thermal conductivity ice-cemented soil or sandstone, the depth to the melting point is kilometers below the surface, while for the low thermal conductivity uncemented dry soil, the depth to melting is between 100 and 200 m, consistent with the source depth for the observed gullies.

To explore this result further, we first ask, what is the effect of lithostatic compression on the thermal conductivity of loose ice-free soil? Densification resulting from particle rearrangement and particle deformation at the grain contacts will both act to increase the thermal conductivity as the lithostatic pressure is increased. Unfortunately, the nature of these effects is not well known. Terrestrial soil data is limited, as liquid water content dominates

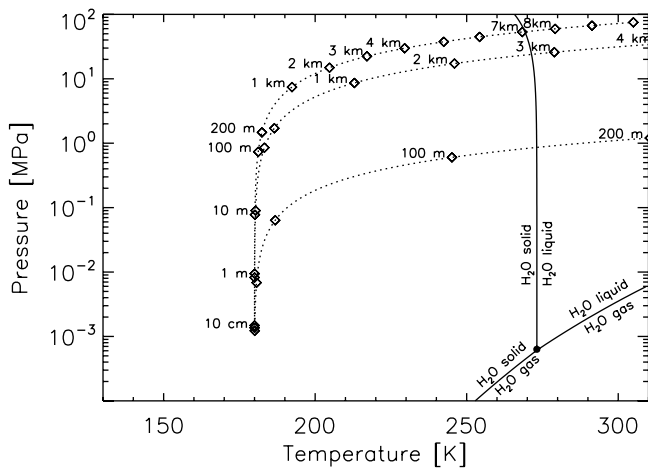


Figure 8. Geothermal pressure-temperature profiles for various thermal conductivities and densities, superimposed on the phase diagram for water. The top profile uses a conductivity of $2.4 \text{ W m}^{-1} \text{ K}^{-1}$ and a density of 2018 kg m^{-3} , consistent with an ice-cemented soil. The middle profile uses a conductivity of $0.9 \text{ W m}^{-1} \text{ K}^{-1}$ and a density of 2338 kg m^{-3} , consistent with a dry sandstone. The bottom profile uses a conductivity of $0.045 \text{ W m}^{-1} \text{ K}^{-1}$ and a density of 1650 kg m^{-3} , consistent with a dry, unconsolidated soil. Properties are assumed constant with depth, with a surface temperature of 180 K and a geothermal heat flux of 30 mW m^{-2} . Depths to the base of the permafrost are several kilometers, except for the dry soil, which acts as a thermal insulator. Water phase information is from *Mellon and Jakosky* [1993] for sublimation, *Iribarne and Godson* [1981] for vaporization, and *Hobbs* [1974] for melting.

the thermal conductivity over these factors. In addition, measurements at 1 bar of gas pressure are not as applicable, since gas conduction at lower Martian pressures plays an important role. Nonetheless, *Woodside and Messmer* [1961] measured the thermal conductivity of an evacuated sandstone under a lithostatic pressure up to 27.5 MPa . For an initial increase in pressure of 1 MPa , they observed a 17% increase in the thermal conductivity, which they attribute to particle deformation resulting in increased grain contact under pressure. As the pressure was raised, the resulting conductivity increase tapered off to a maximum increase of 75% over the initial value. In the absence of applicable data for unconsolidated soils on Mars, we assume a 25% increase in the thermal conductivity due to particle deformation for every 1 MPa of overburden.

Densification will also affect the thermal conductivity. *Clifford* [1993] proposed a model for the porosity of the Martian regolith as decreasing exponentially as a function of depth (a result of overburden compaction) with a characteristic scale length λ of 2820 m . Using this model, the density of the subsurface can be expressed as

$$\rho(Z) = \rho_i(1 - \varepsilon_0 e^{-Z/\lambda}), \quad (7)$$

where ε_0 is the surface porosity, which we assume to be 40%, and ρ_i is the intrinsic density of the regolith minerals, which we assume to be 2750 kg m^{-3} . *Presley and Christensen* [1997b] measured the effects of density on the thermal conductivity of $25\text{--}30 \mu\text{m}$ quartz particles in the absence of an overburden pressure, but at Mars atmospheric pressure. While their data are limited, they found that thermal conductivity increases slightly with density and can be expressed by $k(\rho) = 0.01 + 6.4 \times 10^{-6} \rho \text{ W m}^{-1} \text{ K}^{-1}$ for densities of $700\text{--}1600 \text{ kg m}^{-3}$. Although this relation applies to a narrow particle size range, it expresses a representative dependence on density. To obtain a thermal conductivity profile for the soil subsurface, we adjust this relation for the desired surface value k_0

and increase the thermal conductivity with the pressure and density:

$$k(Z) = k(\rho) \frac{k_0}{k(\rho_0)} [1 + 0.25P(Z)], \quad (8)$$

where ρ_0 is the density at the surface and pressure is expressed in MPa. For a nominal soil profile, (7) and (8) result only in a 50% increase in the thermal conductivity between the surface and 300 m depth.

Aside from geothermal heating, obliquity oscillations will induce oscillations in the mean annual temperature of the surface, which will, in turn, propagate deep into the subsurface. Seasonal temperature oscillations will penetrate $\sim 4 \text{ m}$ into the subsurface (~ 5 times an annual skin depth, $\delta = 1/\rho c \sqrt{\text{period}/\pi}$), while obliquity-driven oscillations with a period of $129,000$ years will penetrate ~ 360 times deeper. Figure 9 shows the geothermal gradient using (7) for density and (8) for the thermal conductivity as a function of depth and solving (5) and (6), with a mean annual surface temperature of 180 K . Figure 9 also shows the magnitude of an obliquity-induced oscillation as a function of depth for a 15 K amplitude oscillation in mean annual surface temperature. It is clear that the depth at which the melting point is encountered can undergo more than 10 m of oscillation.

In Figure 10 we show the depth of the melting isotherm as a function of latitude for obliquity oscillations between 20° and 40° and between 40° and 60° ; surface temperatures used are shown in Figure 3, and Table 2 lists other key parameters. At all latitudes the depth of the melting point falls between about 80 and 215 m with less latitudinal variation at higher obliquities. In Figure 10 the soil is assumed to be relatively structurally uniform above the melting isotherm; only lithostatic effects on conductivity were included. However, observations of cohesive strata indicate that significant layering is present. Larger depths to the melting isotherm would occur if the soil contained layers of high thermal conductivity material such as rock or if the thermal conductivity increased more rapidly with depth than we estimate. For example, if the soil consisted of a low thermal conductivity volcanic ash with 10% of the total depth interspersed with thin layers of high thermal conductivity basaltic lava flows, the flow units would be comparatively isothermal and to first order the depth of the melting isotherm would increase by $\sim 10\%$. Even if as much as 50% of the subsurface contained high-conductivity strata, the depth to the melting isotherm would increase by less than a factor of 2. The

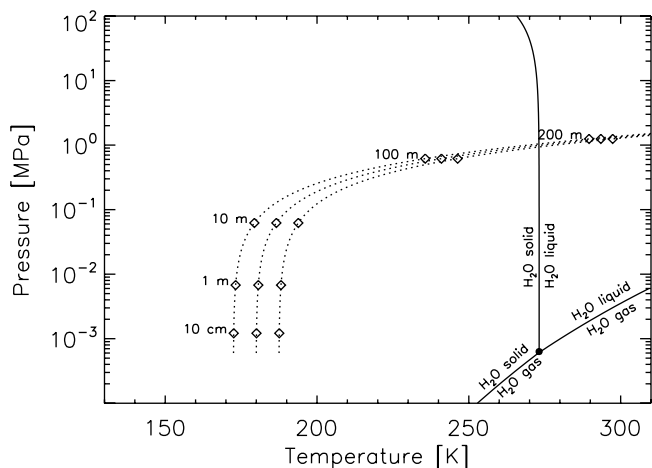


Figure 9. Geothermal pressure-temperature profiles utilizing equations (5)–(8) for an unconsolidated soil. The three profiles represent the mean and the envelope of thermal oscillations due to orbital cycles. The depth to the melting point can vary significantly with obliquity, eccentricity, and L_5 of perihelion.

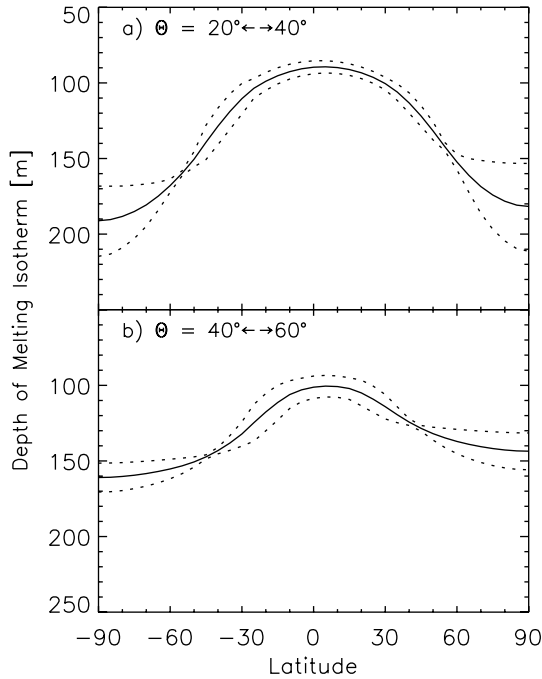


Figure 10. Depth to the melting isotherm as a function of latitude utilizing equations (5)–(8) for properties given in Table 2 and surface temperatures shown in Figure 3. The dotted lines represent the range of depths for obliquity oscillations between (a) 20° and 40° and (b) 40° and 60°. The solid line represents the mean depth.

blanketing nature of low thermal conductivity soil will dominate the increasing temperature with depth.

The addition of a number of thin layers of a competent rock unit can also provide a barrier to the transport of water vapor upward from a potential groundwater table, thus preventing the overlying dry soil from becoming ice-saturated. Under favorable conditions these layers can also act as aquicludes, trapping liquid water in a confined aquifer. We propose a conceptual model in Figure 11, where impermeable rock layers are able to trap water and in this way maintain a dry overlying soil. Observations of gullies suggest that in many cases water may be expelled from beneath or between specific cohesive strata (see, for example, Figure 1). The stability of near-surface ground ice would allow an ice-cemented-soil plug to prevent water from migrating toward the slope, where strata are exposed; the latitudinal distribution of gully features is consistent with the long-term stability of ice-cemented permafrost.

Obliquity-driven oscillations in the subsurface temperatures would cause freezing cycles in the trapped liquid water and would build up fluid pressure that would allow the liquid water to escape to the surface. Carr [1979] suggested a similar mechanism for the eruption of groundwater to form the outflow channels, where a gradual thickening of the permafrost due to long-term climate change caused fluid pressures to increase in the groundwater system. The freezing of water results in a 9% increase in volume, evident by the difference in densities (see Table 2). In a confined aquifer the ice and water will become compressed, resulting in an increase in fluid pressure by the amount

$$P_f = \frac{0.09Ef}{3f(1-2) + EK(1-f)}, \quad (9)$$

where E is Young's modulus for ice, ν is Poisson's ratio for ice, K is the compressibility of liquid water, and f is the fraction of water in the ice phase. If the ice content approaches 100%, the freezing pressure could approach 800 MPa, if confined, greatly exceeding the strength of frozen soil, rock, and the over burden pressure.

Since this pressure would tend to force the strata apart and ice-cemented soil will be the weakest component, it would be most likely for the ice-cemented soil between the strata to fail in tension, allowing liquid water to be expelled onto the surface.

To estimate the amount of water pressure than can be achieved from nominal cycles in the Martian orbit, we employed our thermal model with the inclusion of the orbit shown in Figure 2 to calculate the time history of temperature in the subsurface. We adopt thermal and physical properties given in Table 2 for a latitude of 50° south. We include a 17 m thick layer of water-saturated soil, assumed confined at the top and bottom by impermeable rock layers, centered at a depth of ~ 146 m. The depth is chosen to coincide with the depth at which the long-term average temperature is just above melting, 273 K. The 17 m layer thickness is chosen for numerical convenience. Water is allowed to freeze or thaw depending on the net flux of heat energy in and out of the layer. The temperature history is calculated from 6 Myr ago to the present, discarding the first million years to avoid the effects of initial conditions. Figure 12 shows the resulting mean annual surface temperatures, the mass of ice formed, and the resulting freezing pressure as a function of time. Orbital oscillations (dominated by obliquity) cause oscillations in the mean annual surface temperature, which propagate to the aquifer. Freezing is induced when a cooling wave reaches the aquifer, which results in increasing fluid pressure. Both short-term oscillations and long-term trends in the orbit result in freezing and melting in the aquifer. Freezing pressures will generate stress in the surrounding rock and ice-cemented soil. The necessary alignment of the aquifer with the 273 K isotherm suggests that conditions are not always favorable and that if aquifers are abundant, only a subset of them might be capable of periodic expulsion of water.

The tensile strength of frozen soil on Mars is not known directly. Laboratory measurements of the tensile strength of frozen soil and polycrystalline ice samples typically ranges from 0.5 to 2.6 MPa for a range of temperatures from 233 to 263 K [Lachenbruch, 1962; Tsyrovich, 1975; Hobbs, 1974; Gold, 1978; Schulson et al., 1984], varying with temperature, ice crystal size, and soil content and type. The size of the test sample also affects the measured strength. Weibull theory of the weakest link in a distribution of flaws indicates that the tensile strength of polycrystalline materials should be proportional to $L^{-1/m}$, where L is the length scale and m is a material constant [e.g., Costin, 1987; Bao and Jin, 1993]. Statistically, it is more likely to encounter a weaker point defect the longer the length scale. Values of m typically range from 6 and up [Irwin, 1961], though a value for frozen soil is unknown. Tests are

Table 2. Geothermal Heating of Ground Ice: Model Parameters

Property	Parameter	Value	Units
Geothermal heat flux	q	30	mW m ⁻²
Thermal conductivity ^a	k	0.045	W m ⁻¹ K ⁻¹
Albedo	A	.25	
Surface porosity	ϵ_0	0.4	
Intrinsic density	ρ_i	2750	kg m ⁻³
Dry soil specific heat	C	837	J kg ⁻¹ K ⁻¹
Density of water ^b	ρ_{liquid}	999.8	kg m ⁻³
Density of ice ^b	ρ_{ice}	915.6	kg m ⁻³
Specific heat of water ^c	C_{liquid}	4217.7	J kg ⁻¹ K ⁻¹
Specific heat of ice ^b	C_{ice}	1962	J kg ⁻¹ K ⁻¹
Latent heat of fusion ^b	L	3.335×10^5	J kg ⁻¹
Young's modulus, ice ^b	E	93.3×10^8	Pa
Poisson's ratio, ice ^b	ν	0.325	
Compressibility, water ^c	K	5×10^{-10}	Pa ⁻¹

^a Thermal inertia, thermal conductivity, density, and specific heat are related by $I = \sqrt{k\rho C}$.

^b Petrenko and Whitworth [1999].

^c Weast [1986].

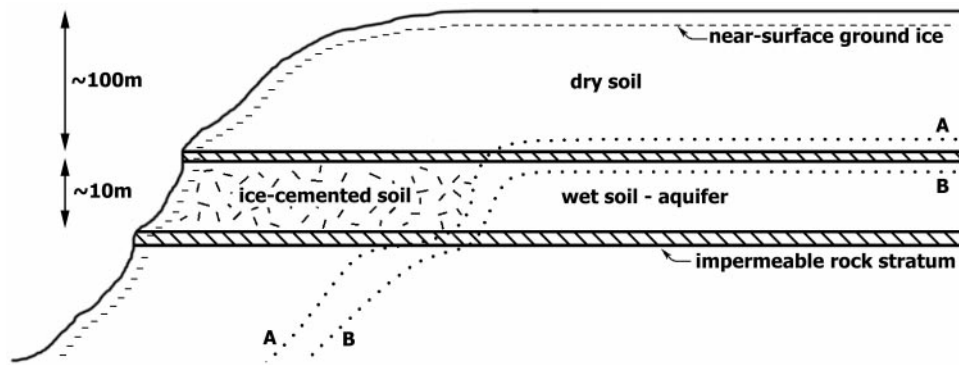


Figure 11. Conceptual model of trapping and freezing of groundwater. Strata of impermeable rock trap a permeable soil unit saturated with water. Toward the slope, water in the aquifer saturates the permafrost with ice, preventing liquid water from escaping. Orbitally driven oscillations in the mean annual surface temperature cause partial freezing of the water in the aquifer, which in turn increases the water pressure until the ice-saturated permafrost fractures, allowing water to escape to the surface. “A” and “B” indicate the position of melting isotherms at different times during orbital cycles. Enclosing the aquifer opposite the slope (on the right, not shown) can be accomplished by a higher thermal conductivity soil layer, upturned rock strata, or gradual merging of the rock units.

typically carried out on samples of order 10 cm in size, while the proposed source aquifer for water forming gullies at the surface may be a kilometer or more in scale. For $m = 10$ the resulting tensile strength would range from 0.2 to 1 MPa. Under similar considerations the tensile strength of basalt would be around 3–5.5

MPa [see *Singh*, 1989]. For comparison, the overburden pressure at 146 m depth would be around 0.9 MPa.

These results suggest that sufficient pressures can be generated by water freezing in an aquifer (as shown in Figure 12) that the frozen soil between the liquid water aquifer and the slope surface

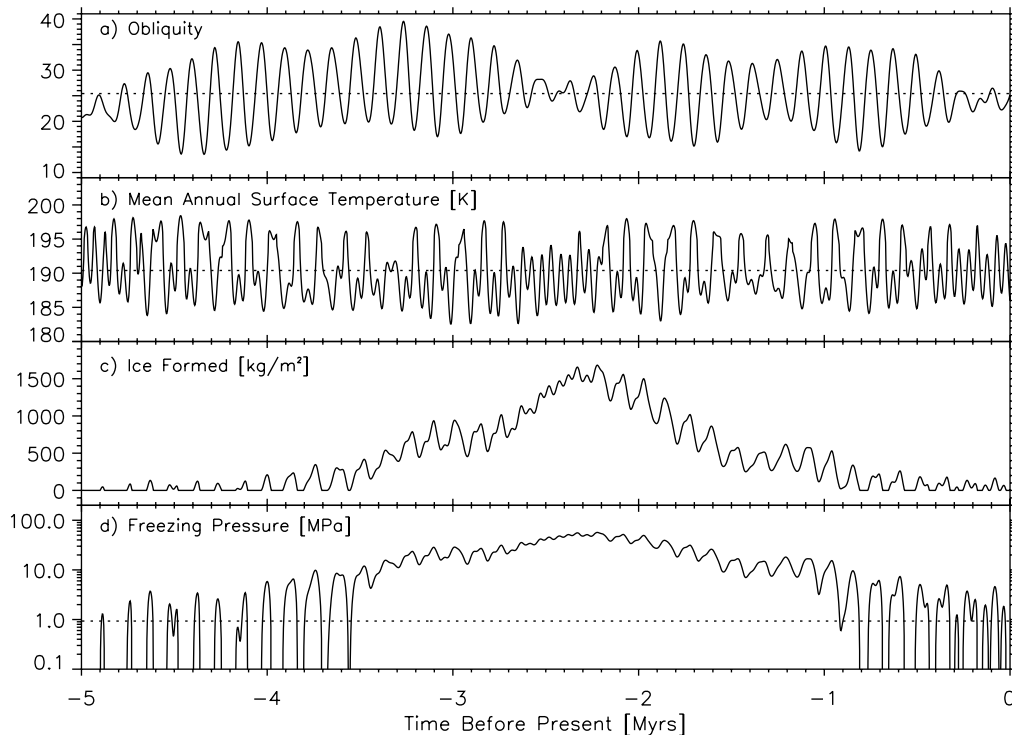


Figure 12. Long-term freezing simulation for 50°S latitude. Shown are (b) mean annual surface temperature, (c) mass of ice formed, (d) the resulting freezing pressure, compared with (a) the obliquity history for the past 5 Myr. The model assumes that a 17 m layer of confined water saturated soil exists at 146 m depth (centered roughly on the 273 isotherm) and assumes the parameters in Table 2. Orbital oscillations cause oscillations in the mean annual surface temperature, which propagate down to the aquifer, inducing freezing and an increase in fluid pressure. Results show that heat flux oscillations from orbital cycles can generate more than sufficient freezing pressures to fracture the ice-cemented permafrost, allowing the water to escape to the surface. Such oscillations occur throughout Martian history. This simulation also predicts non-zero and increasing freezing pressures today. The dotted lines in Figures 12a, 12b, and 12d represent the long-term mean obliquity, the long-term mean surface temperature, and the overburden pressure, respectively.

(see also Figure 11) would fail, overcoming the lithostatic pressure and tensile strength of the ice-cemented soil, potentially allowing water to escape to the surface. Such expulsions of liquid water would have occurred periodically where conditions are favorable throughout Mars' recent history and may even be occurring today; the example calculations used in Figure 12 also predict an increase in freezing pressure in the current epoch. In addition, the peak in the ice buildup and the freezing pressure around 2.3 Myr ago results from a gradual and subtle cooling, corresponding to an increase in the mean obliquity during that time. This cooling is a direct consequence of the assumed orbit model. Subtle uncertainties in the Martian orbit and small deviations in this long-term trend could result in a shift in the peak pressures to other periods in recent Martian history, including today.

The ability of the liquid water to reach the surface will depend on the rate of escape and the rate of freezing within the failure-induced fracture. When the fracture forms in the ice-cemented frozen soil, while it will likely propagate to the surface due to concentration of stress at the crack tip, it might open only a few millimeters, enough to relieve the stress. Water flowing into this small fracture would freeze in place before getting far from the source, creating a short plug of ice near the aquifer in an otherwise long, ice-free crack, and again confining the aquifer. Continued freezing of the aquifer would again build pressure and open the crack further, breaking the short ice plug which is now a zone of weakness. Eventually, the crack would be open enough to allow for a rapid flux of water to the surface of the slope without freezing in the crack. While stress rates are small (0.5 MPa kyr^{-1} in Figure 12), fluid velocities in such a discharge could be quite large and short in duration following abrupt failure of an ice and frozen-soil plug. A more precise determination of the discharge rates requires knowledge of a number of unknown factors, including initial water temperature, size and permeability of the reservoir, and the size and rheological properties of the rock layers. The amount of water expelled will depend on the size of the aquifer and the fraction of freezing that takes place. For example, the 2500 m^3 of water expelled as suggested by *Malin and Edgett* [2000], assuming only 1% of the aquifer freezes, would come from an aquifer containing $2.8 \times 10^6 \text{ m}^3$ of water; assuming 40% porosity and a 20 m aquifer thickness, the areal extent would need to be only about $1/3 \text{ km}^2$. Once water is expelled onto the surface, even a modest discharge forming a small stream 10 cm deep would be able to flow for a few hours in the present Martian climate before completely freezing [*Carr*, 1983].

In our model we present a simple configuration of horizontal strata, or aquicludes, trapping water in an aquifer (Figure 11). Complete confinement of the aquifer water is necessary to build freezing pressures. A number of conditions can occur to trap the water in an aquifer opposite the slope surface (on the right side of Figure 11), such as deformation and upturning of the impermeable rock strata or an increase in the thermal conductivity of the overlying soil with horizontal distance from the slope, in both cases causing a frozen "plug" in the aquifer. In one scenario, water in the shallow aquifer may persist due to a local absence of permeable fractures in an otherwise disrupted rock layer. In the terrain surrounding the impermeable zone, some water may diffuse into the overlying soil, increasing the thermal conductivity and the depth of the melting isotherm. Liquid water can become trapped in this zone where soil above the impermeable rock remains ice-free and the depth to the melting isotherm remains shallow. Such an undisrupted zone need not be large, as discussed above, and may be $<1 \text{ km}^2$. The permeability of these confining strata will need to be low, consistent with unfractured rock, to prevent leaking and allow freezing pressures to build. Furthermore, the permeability of the upper strata can be further reduced by ice occupying any existing pores.

Recharge of a confined aquifer could occur at times of extreme warming (due perhaps to high obliquity or a judicious combination

of orbital elements). A warming trend at the surface would propagate into ground ice adjacent to the aquifer, partly thawing an otherwise confining plug and allowing the aquifer temporary access to a larger source of water. Similarly, small temporal variations in the regional geothermal heat flow could partly thaw the confining ground ice.

A number of striking similarities exist between our proposed mechanism for expelling liquid water to the surface of Mars and the formation and evolution of terrestrial closed-system pingos. On Earth, pingos are large ice-cored hills, typically of order hundreds of meters in diameter, which frequently form in the bottoms of shallow drained lakes [e.g., *Mackay*, 1978; *Washburn*, 1980; *Mackay*, 1998]. After the lake has drained, the saturated lake sediments begin to freeze inward from the top and sides. Pore water is expelled by this freezing process to the near surface in localized areas, where it freezes, forming an ice-cored mound, a pingo. Pingos typically consist of a relatively clean ice core underlain by a lens of liquid water. Pingo growth proceeds as ice from the water lens is added to the core each year. *Mackay* [1977, 1978, 1998] measured the fluid pressure in this water lens and in the surrounding saturated sediments and found that it frequently exceeds the overburden pressure. Pressures are usually highest in late winter and spring, when seasonal freezing propagates to the base of the permafrost at a few tens of meters' depth. Moreover, pingos have been reported to rupture and expel water from the interior. *Mackay* [1998] reported that $\sim 25\%$ of pingos he studied during the a period of ~ 20 years experienced hydrofractures, most commonly at the periphery, where the fluid pressures in the water lens exceeded the tensile strength of the frozen soil, fracturing through to the surface, resulting in springs. *Bogomolov and Sklyarevskaya* [1973] reported observation of two pingos erupting explosively, tossing soil, water, and meter sized blocks of ice meters into the air. Discharge rates vary from $<0.01 \text{ m}^3 \text{ s}^{-1}$ to over $1 \text{ m}^3 \text{ s}^{-1}$ immediately following one of the explosive eruptions; discharges last from hours at higher rates to weeks at lower rates.

Differences are evident between terrestrial closed-system pingos and our proposed mechanism for Martian gullies. Terrestrial pingos occur in relatively shallow permafrost, tens of meters deep, while we propose that shallow Martian permafrost is hundreds of meters deep. Both are driven by freezing cycles caused by temperature oscillations at the surface. At terrestrial permafrost depths, seasonal temperature cycles can cause periodic freezing, while at Martian shallow-permafrost depths, freezing cycles coincide with orbital cycles. However, at the larger depths on Mars, combined with the presence of competent rock strata, water is more easily forced laterally to nearby slopes. Any uplift similar to pingo growth would be dissipated over a wide lateral expanse, making uplift difficult to detect.

5. Additional Discussion and Observational Tests

The most promising sources of water that could result from solar heating of near-surface ground ice are that (1) ice at the ice table melts by conducted heat from the surface or that (2) mass wasting of the top few tens of centimeters of desiccated soil exposes the ice table to direct solar heating. In both cases the maximum temperatures reached by the ice are the highest at the highest possible obliquities but still below the melting point of pure water. Depending on the obliquity and salt species, roughly 15–40% salt is required in the ice for melting to occur. Most salts species (except sulfates) that have been suggested for Mars would be sufficient (see Figure 7). The occurrence of salts in these quantities may be detectable in evaporite deposits at the base of the gullies and distributary fans. Most of these salts would be white and high albedo in appearance, if deposited in a fine crystalline form, and could be visible in imaging data, though no such appearance has been reported. Depending on the species and the spatial extent of

such a deposit, they may also be detectable in spectroscopic data. The detection of salt deposits at the depositional base of the gullies, however, would not be conclusive evidence for melting of salty ground ice, as groundwater in a confined aquifer could also contain soluble salts.

In addition, melting of salty near-surface ground ice is not consistent with the observed gully properties. Gullies are observed to occur poleward of $\sim 30^\circ$ latitude; however, at higher obliquity, near-surface ground ice should be present globally [Mellon and Jakosky, 1995], populated by condensation of atmospheric water in the top few meters. The presence of salts in the equatorial soil would promote the melting of ground ice in the same way as at higher latitudes, yet gullies are not observed in these regions. Gullies are also observed to preferentially occur on poleward facing slopes. Results indicate that melting of salty ground ice should be independent of slope angle and orientation, since maximum temperatures experienced by the ice table are slope independent (Figure 6). Also, near-surface ground ice should be present on all slopes at higher obliquities, for reasons similar to being present at all latitudes, as discussed above. Therefore gullies forming from melting of salty near-surface ice should not be expected to show any slope orientation preference. Finally, while a confined salt deposit might result in ground ice preferentially melting at a narrow band below the top of the slope, such a salt deposit could occur at any depth along the slope surface and would not be limited to a few hundred meters below the top of the slope. In general, the lack of consistency between the salty near-surface ice model and observed gully properties leads us to rule out this mechanism.

Our results from the geothermal model suggest that the base of the permafrost could be more shallow than previously considered (a few hundred meters or less) due to the blanketing nature of an unconsolidated and ice-free soil layer above. However, numerous layers of rock, including additional completely frozen confined aquifers, can also be present; the relative fractions of dry soil and rock will depend on the thermal conductivities of each unit, but as much as 50% rock layers will increase the depth of the melting isotherm only by a factor of 2 or less. In either case a volcanic or other subsurface concentration of geothermal heat is not required for liquid water to persist close to the surface in regions where gullies are observed. Future subsurface sounding (electromagnetic or seismic) on the level surfaces above the slope may be required to place constraints on the density, structure, and possible presence of liquid water at relatively shallow depths. At these depths, liquid water would be more accessible via these techniques than previously considered.

Groundwater on Mars is likely to contain some quantity of soluble minerals through its interaction with the regolith [e.g., Fanale, 1976; Kuzmin, 1983; Clifford, 1990; Kuzmin and Zabalueva, 1998]. Water in a confined aquifer may similarly contain soluble salts supplied directly from a groundwater system and possibly enhanced by concentration during partial freezing within the permafrost [Kuzmin and Zabalueva, 1998]. The presence of a brine aquifer would not greatly affect its ability to generate freezing pressure and erupt onto the surface. The resulting reduction in the freezing point would allow the thermal conductivity of the overburden to be larger, while achieving the same depth to the melting isotherm. For example, assuming a relatively large 40 K freezing point depression, the thermal conductivity would need to be increased by a factor of 1.5–2 (depending on the mean annual surface temperature) to reach the melting point at the same depth as with pure water. Since thermal conductivity varies exponentially between geologic materials, such higher values are still low and would require the thermal blanketing effects of an unconsolidated soil.

The geothermal model is consistent with the observation of gullies poleward of 30° latitude. The long-term stability of ground ice in the near surface (the top few meters) is a necessary

condition for containment of the aquifer. Averaged over many obliquity cycles, ground ice in the equatorial region is unstable, and a net loss of ground ice and groundwater will occur [Mellon *et al.*, 1997]. In these regions where ground ice is unstable, the confining ground ice plug (Figure 11) will sublimate into the atmosphere and eventually desiccate the aquifer. Conversely, at higher latitudes, $>30^\circ$ ground ice is stable, and water in an aquifer would persist. In addition, at lower latitudes, equatorward facing slopes will be warmer than poleward facing slopes and less likely to preserve near-surface ground ice, making gullies more difficult to form by this mechanism. At higher latitudes a north-south asymmetry in the abundance of gully features would be difficult to explain, as the confining ground ice would be stable on all slope orientations. Malin and Edgett [2000] do not report the latitudinal dependence on the slope asymmetry; evaluating these dependencies will require better observational statistics and can further test our proposed model.

Figure 10 indicates that the depth of the melting isotherm depends on latitude and that the magnitude of the obliquity-induced oscillations in the depth approaches a minimum in the middle latitudes, varying somewhat with the range of obliquities and the influences of the other orbital elements. If our model is correct, then we would expect a latitudinal dependence in the apparent depth of the source of water and in the frequency of occurrence of gully features; however, the latitudinal dependence in the apparent depth may be subdued by geographic variations in the thermal properties of the soil.

6. Summary

We evaluated two mechanisms for the generation of liquid water at the surface of Mars in its present climate in relation to the formation of gully landforms recently discovered. The first involves melting of near-surface ground ice by solar heating and conduction from the surface. The second involves melting (and refreezing) of water at the base of the permafrost by geothermal heating. We employed standard numerical models of ground temperatures and ground ice stability.

In the first mechanism we consider if (1) ground ice at the top of the ice table can be melted from conducted heat from the surface, (2) seasonal trace quantities of ground ice above the ice table can melt and in enough quantity, and (3) ground ice exposed by erosion of the dry soil layer above the ice table can be melted by direct solar heating. While poleward facing slopes are colder than equatorward facing slopes, slope angle does not greatly affect the maximum temperatures experienced at the top of the ice table, because the depth of ice stability changes with the temperature regime to correspond to the atmospheric water vapor as a primary boundary condition. Trace amounts of ice occur seasonally above the ice table but sublimate rapidly when warmed. Slumping may expose underlying ice-cemented ground; however, exposed ground will be cold, and solar heating will cause desiccation to a depth of 5–10 cm before melting temperatures can be reached. Ice temperatures in all three cases do not reach the melting point (273 K) even at extreme obliquities. Temperatures are high enough at higher obliquities to melt ice if salts are present within the ice. Concentrations of salts required are of order 15–40%. These salt concentrations could leave high-albedo deposits at the surface, which have not been reported in proximity to the gully features. While melting ground ice caused by the presence of salts cannot generally be ruled out, we rule out this model in the formation of the gullies, since it is inconsistent with the latitudinal and slope distribution of observed gullies.

The second mechanism we consider involves preserving pockets of liquid water at shallow depths by normal geothermal heating. We find that global-average geothermal heat can raise subsurface temperatures above the melting point of pure water at depths

consistent with the emergence of gully features if the overlying regolith exhibits a low thermal conductivity at depth. This result is fairly robust, since other parameters (heat flow, density, etc.) can be varied without significant impact; thermal conductivity varies by orders of magnitude for geologic materials, dominating the subsurface temperature profile. This low thermal conductivity is consistent with observations of the thermal inertia of the surface layer and would require a limited amount of compaction, induration, and ice cementing at depth. Layering is evident in the observations, and layers of ice-free, unconsolidated soil would provide the necessary blanketing effect, even when interspersed with high-conductivity rock layers. Upward departures from the average geothermal heat flow are not required. Oscillations in the Martian orbit can drive freeze thaw cycles at depth, and if water is trapped between relatively impermeable layers, water may be forced to the surface under freezing pressure, similar to springs emanating from terrestrial pingos. Such cycles are capable of forcing water to the surface today. We favor this mechanism since it is consistent with the latitudinal distribution and preferred slope orientation of the observed gullies. Further observations can be made to evaluate and refine this model.

Acknowledgments. We would like to thank Bruce Bills, Mark Bullock, Josh Colwell, Ken Edgett, Bruce Jakosky, Shannon Pelkey, Marsha Presley, and Steve Ruff for helpful discussions. This work was supported by NASA's Planetary Geology and Geophysics Program through grants NAG5-8910 and NAG5-4448. RJP would like to thank LASP and SWRI in Boulder for their hospitality.

References

- Bao, Y., and Z. Jin, Size effects and a mean-strength criterion for ceramics, *Fatigue Fract. Eng. Mater. Struct.*, **16**, 829–835, 1993.
- Bills, B. G., The rigid body obliquity history of Mars, *J. Geophys. Res.*, **95**, 14,137–14,153, 1990.
- Binder, A. B., R. E. Arvidson, E. A. Guinness, K. L. Jones, E. C. Morris, T. A. Mutch, D. C. Pieri, and C. Sagan, The geology of the Viking Lander 1 site, *J. Geophys. Res.*, **82**, 4439–4451, 1977.
- Bogomolov, N. S., and A. N. Sklyarevskaya, On explosion of hydrolaccoliths in southern part of Chitinskaya Oblast, in *Siberian Nelads*, translated from Russian, edited by V. R. Alekseyev et al., U.S. Army Cold Reg. Res. and Eng. Lab., *Draft Transl. 399*, pp. 187–191, Hanover, N. H., 1973.
- Brass, G. W., Stability of brines on Mars, *Icarus*, **42**, 20–28, 1980.
- Carr, M. H., Formation of Martian flood features by release of water from confined aquifers, *J. Geophys. Res.*, **84**, 2995–3007, 1979.
- Carr, M. H., Stability of streams and lakes on Mars, *Icarus*, **56**, 476–495, 1983.
- Clark, B. C., and D. C. van Hart, The salts of Mars, *Icarus*, **45**, 370–378, 1981.
- Clark, B. C., A. K. Baird, R. J. Weldon, D. M. Tsusaki, L. Schnabel, and M. P. Candelaria, Chemical composition of Martian fines, *J. Geophys. Res.*, **87**, 10,059–10,067, 1982.
- Clifford, S. M., The role of thermal vapor diffusion in the subsurface hydrological evolution of Mars, *Geophys. Res. Lett.*, **18**, 2055–2058, 1990.
- Clifford, S. M., A model for the hydrological and climatic behavior of water on Mars, *J. Geophys. Res.*, **98**, 10,973–11,016, 1993.
- Costin, L. S., Time-dependent deformation and failure, in *Fracture Mechanics of Rock*, edited by B. K. Atkinson, pp. 167–216, Academic, San Diego, Calif., 1987.
- Davies, G. F., and R. E. Arvidson, Martian thermal history, core segregation, and tectonics, *Icarus*, **45**, 339–346, 1981.
- Fanale, F. P., Martian volatiles: Their degassing history and geochemical fate, *Icarus*, **28**, 179–202, 1976.
- Fanale, F. P., J. R. Salvail, A. P. Zent, and S. E. Postawko, Global distribution and migration of subsurface ice on Mars, *Icarus*, **67**, 1–18, 1986.
- Farmer, C. B., and P. E. Doms, Global and seasonal variations of water vapor on Mars and the implications for permafrost, *J. Geophys. Res.*, **84**, 2881–2888, 1979.
- Folkner, W. M., C. F. Yoder, D. N. Yuan, E. M. Standish, and R. A. Preston, Interior structure and seasonal mass redistribution of Mars from radio tracking of Mars Pathfinder, *Science*, **278**, 1749–1752, 1997.
- Franck, S., and I. Orgzall, A new view of Martian evolution, *Earth Moon Planets*, **37**, 287–313, 1987.
- Gold, L. W., Ice pressures and bearing capacity, in *Geotechnical Engineering for Cold Regions*, edited by O. B. Andersland and D. M. Anderson, pp. 216–275, McGraw-Hill, New York, 1978.
- Haberle, R. M., and B. M. Jakosky, Atmospheric effects on the remote determination of thermal inertia on Mars, *Icarus*, **90**, 187–204, 1991.
- Hall, R. E., and M. S. Sherrill, Freezing-point lowerings of aqueous solutions, in *International Critical Tables, vol. VI*, edited by E. W. Washburn, pp. 254–264, McGraw-Hill, New York, 1928.
- Hobbs, P. V., *Ice Physics*, Oxford Univ. Press, New York, 1974.
- Horne, R. A., *Marine Geochemistry*, John Wiley, New York, 1969.
- Iribarne, J. V., and W. L. Godson, *Atmospheric Thermodynamics*, D. Reidel, Norwell, Mass., 1981.
- Irwin, G. R., Effects of size and shape in fracture of solids, in *Properties of Crystalline Solids, ASTM Spec. Tech. Publ.*, **283**, 118–128, 1961.
- Jakosky, B. M., and E. S. Barker, Comparison of ground-based and Viking orbiter measurements of Martian water vapor: Variability of the seasonal cycle, *Icarus*, **57**, 322–334, 1984.
- Jakosky, B. M., and C. B. Farmer, The seasonal and global behavior of water vapor in the Martian atmosphere: Complete global results of the Viking atmospheric water detector experiment, *J. Geophys. Res.*, **87**, 2999–3019, 1982.
- Jakosky, B. M., B. G. Henderson, and M. T. Mellon, The Mars water cycle at other epochs: Recent history of the polar caps and layered terrain, *Icarus*, **102**, 286–297, 1993.
- Jakosky, B. M., B. G. Henderson, and M. T. Mellon, Chaotic obliquity and the nature of the Martian climate, *J. Geophys. Res.*, **100**, 1579–1584, 1995.
- Johnston, D. H., T. R. McGetchin, and M. N. Toksöz, The thermal state and internal structure of Mars, *J. Geophys. Res.*, **79**, 3959–3971, 1974.
- Kuzmin, R. O., *The Cryolithosphere of Mars*, Izdatel'stvo Nauka, Moscow, 1983.
- Kuzmin, R. O., and E. V. Zabalueva, On salt solutions in the Martian cryolithosphere, *Sol. Syst. Res.*, **32**, 187–197, 1998.
- Lachenbruch, A. H., Mechanics of thermal contraction cracks and ice-wedge polygons in permafrost, *Spec. Pap. Geol. Soc. Am.*, **70**, 69 pp., 1962.
- Laskar, J., Secular evolution of the solar system over 10 million years, *Astron. Astrophys.*, **198**, 341–362, 1988.
- Laskar, J., A numerical experiment on the chaotic behavior of the solar system, *Nature*, **338**, 237–238, 1989.
- Laskar, J., and P. Robutel, The chaotic obliquity of the planets, *Nature*, **361**, 608–612, 1993.
- Leighton, R. B., and B. C. Murray, Behavior of carbon dioxide and other volatiles on Mars, *Science*, **153**, 136–144, 1966.
- Linke, W. F., *Solubilities of Inorganic and Metal-Organic Compounds*, D. Van Nostrand, Princeton, N. J., 1958.
- Mackay, J. R., Permafrost growth and superpermafrost pore water expulsion, Tuktoyaktuk Peninsula, District of Mackenzie, *Pap. 77-1A*, pp. 323–326, Geol. Surv. of Can., Ottawa, Ontario, Canada, 1977.
- Mackay, J. R., Sub-pingo water lenses, Tuktoyaktuk Peninsula, Northwest Territories, *Can. J. Earth Sci.*, **15**, 1219–1227, 1978.
- Mackay, J. R., Pingo growth and collapse, Tuktoyaktuk Peninsula area, western arctic coast, Canada: A long-term field study, *Geogr. Phys. Quat.*, **52**, 271–323, 1998.
- Malin, M. C., and K. S. Edgett, Evidence for recent ground water seepage and surface runoff on Mars, *Science*, **288**, 2330–2335, 2000.
- Mellon, M. T., and B. M. Jakosky, Geographic variations in the thermal and diffusive stability of ground ice on Mars, *J. Geophys. Res.*, **98**, 3345–3364, 1993.
- Mellon, M. T., and B. M. Jakosky, The distribution and behavior of Martian ground ice during past and present epochs, *J. Geophys. Res.*, **100**, 11,781–11,799, 1995.
- Mellon, M. T., B. M. Jakosky, and S. E. Postawko, The persistence of equatorial ground ice on Mars, *J. Geophys. Res.*, **102**, 19,357–19,369, 1997.
- Mellon, M. T., B. M. Jakosky, H. H. Kieffer, and P. R. Christensen, High-resolution thermal inertia mapping from the Mars Global Surveyor thermal Emission Spectrometer, *Icarus*, **148**, 437–455, 2000.
- Moore, H. J., R. E. Hutton, G. D. Clow, and C. R. Spitzer, Physical properties of the surface materials at the Viking landing sites on Mars, *U.S. Geol. Surv. Prof. Pap.*, **1389**, 1987.
- Moore, H. J., D. B. Bickler, J. A. Crisp, H. J. Eisen, J. A. Gensler, A. F. C. Haldemann, J. R. Matijevic, L. K. Reid, and F. Pavlics, Soil-like deposits observed by Sojourner, the Pathfinder rover, *J. Geophys. Res.*, **104**, 8729–8746, 1999.
- Mutch, T. A., R. E. Arvidson, A. B. Binder, E. A. Guinness, and E. C. Morris, The geology of the Viking Lander 2 site, *J. Geophys. Res.*, **82**, 4452–4467, 1977.
- Paige, D. A., The thermal stability of near-surface ground ice on Mars, *Nature*, **356**, 43–45, 1992.
- Palluconi, F. D., and H. H. Kieffer, Thermal inertia mapping of Mars for 60°S to 60°N, *Icarus*, **45**, 415–426, 1981.

- Petrenko, V. F., and R. W. Whitworth, *Physics of Ice*, Oxford Univ. Press, New York, 1999.
- Presley, M. A., and P. R. Christensen, Thermal conductivity measurements of particulate materials, 2, Results, *J. Geophys. Res.*, *102*, 6551–6566, 1997a.
- Presley, M. A., and P. R. Christensen, The effect of bulk density and particle size sorting on the thermal conductivity of particulate materials under Martian atmospheric pressures, *J. Geophys. Res.*, *102*, 9221–9229, 1997b.
- Rieder, R., T. Economou, H. Wänke, A. Turkevich, J. Crisp, J. Brückner, G. Dreibus, and H. Y. McSween, The chemical composition of Martian soil and rocks returned by the mobile Alpha Proton X-ray Spectrometer: Preliminary results from the X-ray mode, *Science*, *278*, 1771–1774, 1997.
- Rosbacher, L. A., and S. Judson, Ground ice on Mars: Inventory, distribution, and resulting landforms, *Icarus*, *45*, 39–59, 1981.
- Roy, R. F., A. E. Beck, and Y. S. Touloukian, Thermophysical properties of rocks, in *Physical Properties of Rocks and Minerals*, edited by C. Y. Ho et al., pp. 409–502, Taylor and Francis, Philadelphia, Pa., 1989.
- Schubert, G., and T. Spohn, Thermal history of Mars and the sulfur content of its core, *J. Geophys. Res.*, *95*, 14,095–14,104, 1990.
- Schubert, G., S. C. Solomon, D. L. Turcotte, M. J. Drake, and N. H. Sleep, Origin and thermal evolution of Mars, in *Mars*, edited by H. H. Kieffer et al., pp. 147–183, Univ. of Ariz. Press, Tucson, 1992.
- Schulson, E. M., P. N. Lim, and R. W. Lee, A brittle to ductile transition in ice under tension, *Philos. Mag. A*, *49*, 353–363, 1984.
- Singh, M. M., Strength of rock, in *Physical Properties of Rocks and Minerals*, edited by C. Y. Ho et al., pp. 83–122, Taylor and Francis, Philadelphia, Pa., 1989.
- Spohn, T., Mantle differentiation and the thermal evolution of Mars, Mercury and Venus, *Icarus*, *90*, 222–236, 1991.
- Stevenson, D. J., T. Spohn, and G. Schubert, Magnetism and thermal evolution of terrestrial planets, *Icarus*, *54*, 466–489, 1983.
- Toksöz, M. N., and A. T. Hsui, Thermal history and evolution of Mars, *Icarus*, *34*, 537–547, 1978.
- Toksöz, M. N., A. T. Hsui, and D. H. Johnston, Thermal evolution of the terrestrial planets, *Moon Planets*, *18*, 281–320, 1978.
- Toon, O. B., J. B. Pollack, W. Ward, J. A. Burns, and K. Bilski, The astronomical theory of climate change on Mars, *Icarus*, *44*, 552–607, 1980.
- Touma, J., and J. Wisdom, The chaotic obliquity of Mars, *Science*, *259*, 1294–1297, 1993.
- Tsyтович, N. A., *The Mechanics of Frozen Ground*, Scripta, McGraw-Hill, New York, 1975. (translation of *Mekhanika Merzlykh Gruntov*, Vysshaya Shkola Press, Moscow, 1973)
- Turcotte, D. L., F. A. Cooke, and R. J. Willeman, Parameterized convection within the Moon and terrestrial planets, *Proc. Lunar Planet. Sci. Conf. 10th*, 2375–2392, 1979.
- Ward, W. R., Climatic variations on Mars, 1, Astronomical theory of insolation, *J. Geophys. Res.*, *79*, 3375–3386, 1974.
- Washburn, A. L., *Geocryology: A Survey of Periglacial Processes and Environments*, John Wiley, New York, 1980.
- Weast, R. C. (Ed.), *CRC Handbook of Chemistry and Physics*, 67th ed., p. B-82, CRC Press, Boca Raton, Fla., 1986.
- Woodside, W., and J. H. Messmer, Thermal conductivity of porous media, II, Consolidated rocks, *J. Appl. Phys.*, *12*, 1699–1706, 1961.
- Zent, A. P., F. P. Fanale, J. R. Salvail, and S. E. Postawko, Distribution and state of H₂O in the high-latitude shallow subsurface of Mars, *Icarus*, *67*, 19–36, 1986.

M. T. Mellon and R. J. Phillips, Laboratory for Atmospheric and Space Physics, University of Colorado, Duane Physics Building, Campus Box 392, Boulder, CO 80309-1711, USA. (mellon@argyre.colorado.edu)

(Received November 9, 2000; revised April 27, 2001; accepted June 5, 2001.)